Materials Today Communications 32 (2022) 104164

Contents lists available at ScienceDirect

Materials Today Communications

journal homepage: www.elsevier.com/locate/mtcomm

Damage localization on CFRP composites by electrical impedance tomography

Helena Rocha [a,b,*], Christophe Fernandes [c], Nelson Ferreira [c], Ugo Lafont [d], João P. Nunes [a]

[a] Institute for Polymers and Composites, University of Minho, Guimarães, Portugal
[b] PIEP – Innovation in Polymer Engineering, Guimarães, Portugal
[c] Stratosphere, Guimarães, Portugal
[d] European Space Research and Technology Centre, European Space Agency, Noordwijk, the Netherlands

ARTICLE INFO

Keywords:
Electrical Impedance Tomography
Boundary Electrodes
Impact Damage Detection
Barely Visible Impact Damage
Carbon Fibre Reinforced Polymer Composite

ABSTRACT

This work exploited the use of electrical impedance tomography (EIT) with one-step difference Gaussian-Newton (GN) algorithm to detect different types of damage on unidirectional carbon fibre/epoxy composite laminates. The major challenge concerning the implementation of EIT on composite materials has to do with their anisotropy. To assess this issue, this study was conducted on carbon fibre composites having different layup configurations with different degrees of anisotropy: a quasi-isotropic layup, to approximate as much as possible these layered materials to an isotropic material, and an unbalanced layup, with further degree of anisotropy. Damage detection in the highly anisotropic unbalanced laminates is a major challenge for EIT technique, which has not been assessed before in the literature. Severe damage, in the form of through-thickness holes, was created in the laminates with different diameters and at two locations of the specimen to evaluate the sensitivity of this technique to damage size and its capacity to detect multiple damages. EIT showed progressive decrease of electrical conductivity as the diameter of through-thickness holes increased. Impact damages of different severities were also created. The EIT technique was able to distinguish different damage shapes in the laminates with different anisotropy. EIT identified elongated shaped damages, produced by impact events of different impact energies, on unbalanced laminates. However, the EIT images overestimate the damaged area, as compared to non-destructive ultrasonic inspections. The EIT images of the quasi-isotropic laminates revealed damage in the central area of the specimens, but a well-defined damage shape could not be distinguished.

1. Introduction

Carbon fibre reinforced polymer (CFRP) composites have increased their presence in structural applications for aerospace and aeronautic applications [1]. The popularity of CFRP materials for such applications can be mainly credited to their light weight and, mostly, to the high specific strength and modulus of carbon fibres used. Yet, multiple, and diverse failure mechanisms may occur simultaneously on fibre reinforced polymer (FRP) composites, making failure prediction an arduous task [2]. FRP composites are particularly affected by low velocity impact (LVI) events, which produce barely visible impact damage (BVID) that may be undetected in maintenance operations [3,4]. BVID on polymer composites is usually caused by a combination of failure mechanisms that can absorb a good amount of energy: delaminations, matrix cracking and fibre breakage [5,6]. Delaminations are characterized by debonding of adjacent laminas having different fibre orientations, leading to severe strength reduction [7].

Different methodologies for structural health monitoring, damage detection and localization for composite structures have been explored in the literature. Although different types of sensors are well developed, such as optical fibre-based sensors and piezoelectric sensors, there is need for such sensors to be embedded in the composite structure during manufacturing and leading to potential effect on the mechanical performance of such structures [8]. Besides, composite instrumentation with embedded optical fibre-based sensors has a reduced successful rate, due to the fragility of the optical fibres [9].

The EIT technique reconstructs tomographic images of the spatial electrical conductivity distribution. Instead of intrusive sensors, EIT uses surface electrodes. A number of electrodes is mounted along the boundary of the electrical conductive composite part, where current is

* Corresponding author at: Institute for Polymers and Composites, University of Minho, Guimarães, Portugal.
E-mail address: helenarocha@dep.uminho.pt (H. Rocha).

https://doi.org/10.1016/j.mtcomm.2022.104164
Received 4 May 2022; Received in revised form 28 July 2022; Accepted 1 August 2022
Available online 2 August 2022

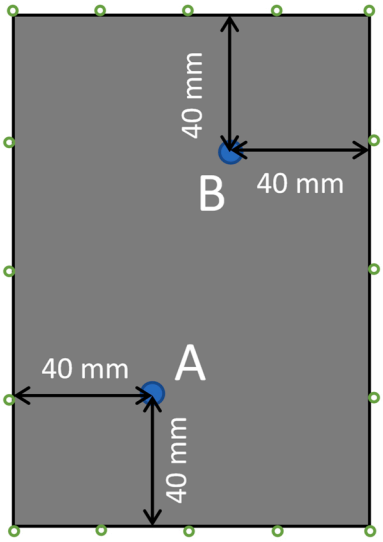

Fig. 1. Schematic representation of the locations of through-thickness holes A and B, having progressively larger diameters of 2, 4.5 and 6 mm. The green dots represent the location of the electrodes contact with the CFRP for EIT measurement.

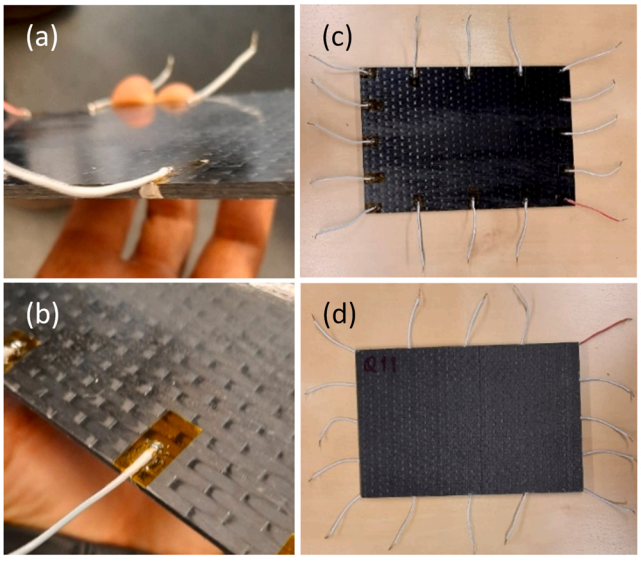

Fig. 2. Boundary electrodes configuration: (a) electrical connection of a boundary electrode at the thickness of the specimen, (b) electrical insulation and fixation of the electric wire on the top surface of the specimen, (c) top surface of a quasi-isotropic specimen subjected to an impact, and (d) bottom surface of the same specimen. Note that the electric wires were facing upwards during impact testing and drilling to avoid detachment.

injected through one pair of electrodes, and the resulting voltages at the remainder consecutive pairs of electrodes are measured [10]. The implementation of EIT in polymer composites is limited to carbon fibre composites and conductive nanoparticle containing composites, such as glass fibre composites having carbon black, carbon nanotubes or metal-based particles modified matrices [11–14]. The application of EIT to monitor anisotropic materials such as composites is still at a low technology readiness level (TRL) and has only recently been exploited in the literature. Recently published works [11,12,15,16] have shown the capability of EIT for the detection and localization of laboratory made damages on FRP composites, such as through-thickness holes, surface cuts, drill rivets, implanted razor blades, and local indentations. Despite

Fig. 3. Electrical impedance tomography equipment.

of its poor spatial resolution, EIT is susceptible to minor conductivity variations [17], which makes it a promising technique for detection of damages that would disrupt the conductive network, including cracks and delaminations created during low velocity impact events.

This study evaluates the suitability of EIT with one-step difference Gaussian-Newton (GN) algorithm to detect different types of damage: through-thickness holes and impact damage with different severities, as created by impact events with different impact energies. Through-thickness holes were created with different diameters and at two locations of the specimen to evaluate the capability of EIT to detect multiple defects and its sensitivity to defect size. Differently from the studies reported in the literature, which use twill or plain fabrics [12, 15–19], the present work was conducted on unidirectional carbon fibre fabrics, having different layup configurations. It is relevant to study composites with this fabric construction, as these are frequently used in advanced application, such as aerospace and aeronautics. Unidirectional fibres are expected to contribute to higher anisotropy than twill or plain fabrics. Two different layup laminates were produced by vacuum assisted resin infusion (VARI): a quasi-isotropic laminate, which is expected to present closer characteristics to an isotropic material, and an unbalanced laminate, having more fibre layers in one orthogonal direction, contributing to an additional level of anisotropy that EIT has never assessed before in the literature. The performance of EIT to detect damage on those laminates was compared. Non-destructive ultrasonic C-scan was used as a control technique for damage detection.

2. Theoretical background

2.1. Drop-weight impact testing

Impact damage is imposed by an out-of-plane localized impact by a drop weight impact setup, following ASTM D7136 standard [20]. The impactor contact force on the laminate, the consequent laminate displacement and absorbed energy can be assessed to evaluate the stiffness and the produced damage in the laminate.

The contact force imposed on the specimen surface by the impactor head is recorded against time for every impact event. The impact velocity, displacement, and absorbed energy, against time, are determined, according to Eqs. 1, 2 and 3, respectively.

$$v(t) = v_i + gt - \int_o^t \frac{F(t)}{m} dt \quad (1)$$

being $v(t)$ the impactor head velocity at time t, v_i the initial impactor head velocity, g the gravitational acceleration, $F(t)$ the recorded load at

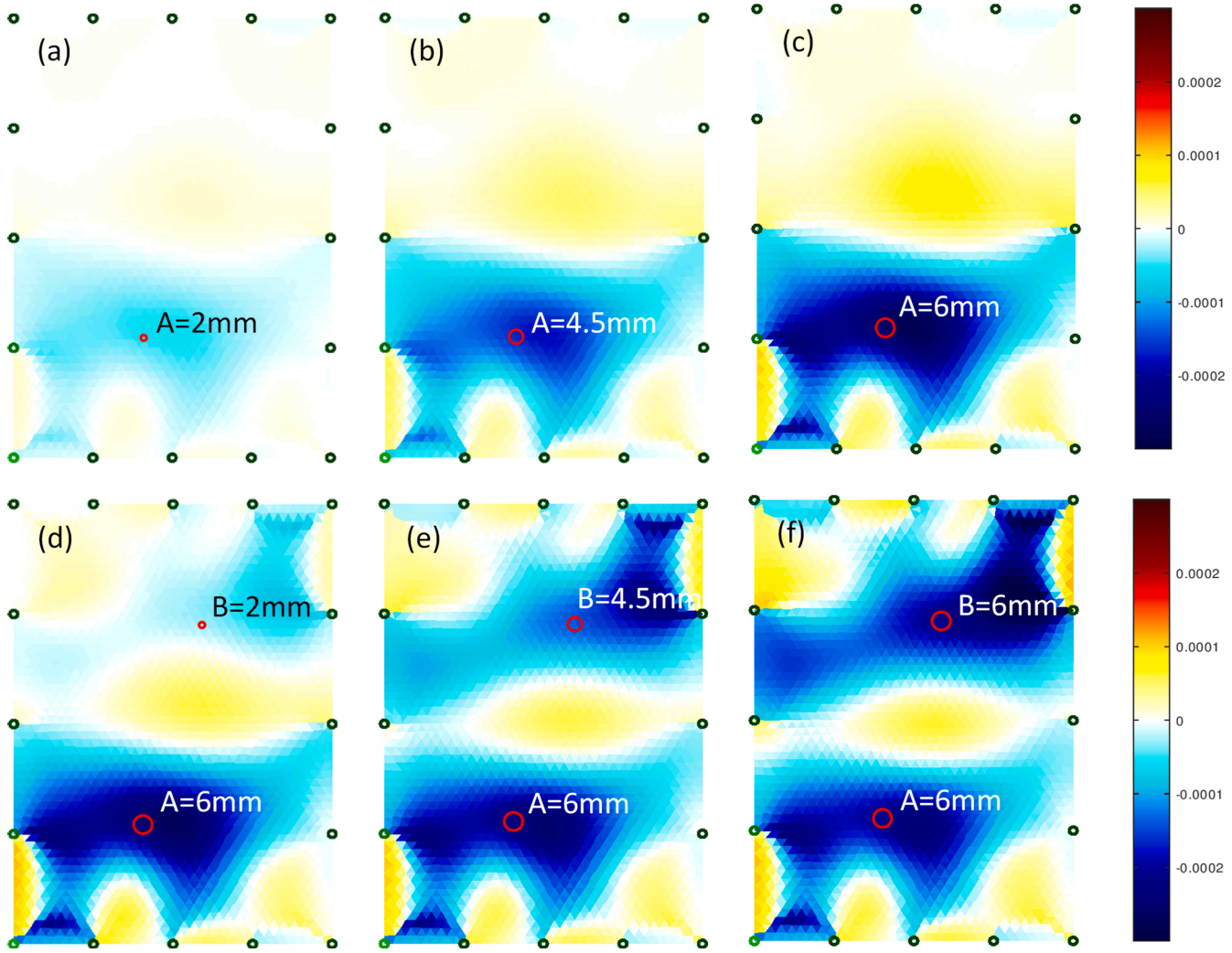

Fig. 4. Reconstructed EIT images using GN algorithm of a quasi-isotropic specimen with through-thickness holes A and B of different diameters: (a) A: 2 mm; (b) A: 4.5 mm; (c) A: 6 mm; (d) A: 6 mm, B: 2 mm; (e) A: 6 mm, B: 4.5 mm; (f) A: 6 mm, B: 6 mm. The green dots represent the connection points of each electrode.

time *t and m* the impactor head mass.

$$\delta(t) = \delta_0 + v_i t + \frac{gt^2}{2} - \int_o^t \int_o^t \frac{F(t)}{m} dtdt \tag{2}$$

being $\delta(t)$ the impactor head displacement at time *t*, and δ_0 the impactor head displacement from the reference position.

$$E_a(t) = \frac{m\left(v_i^2 - v(t)^2\right)}{2} + mg\delta(t) \tag{3}$$

being $E_a(t)$ the absorbed impact energy by the laminate at time *t*.

2.2. Electrical impedance tomography

Static electrical impedance tomography reconstruction algorithms can have some measurement errors, as EIT is more sensitive to changes close to the boundary than to changes happening within the medium. A minor error on the electrode positioning may produce the same voltage measurements as a severe inhomogeneity found in the middle of the medium. Dynamic imaging reconstruction algorithms are good alternatives, where a conductivity image at instant t_2 is calculated from the difference of voltage data v_2 at that instant and the previous measured voltage data v_1 at time t_1 [21]. Imaging can be regarded as a linear problem, using an algorithm for difference EIT. Difference data, *y*, from difference EIT is calculated according to Eq. 4 [22].

$$[y]_i = [v_2]_i - [v_1]_i \tag{4}$$

The conductivity of the medium is modelled through a finite element model, which decomposes it into n_N elements, represented by the conductivity vector $\sigma \in \mathbb{R}^{n_N}$. The vector of conductivity change *x* can also be calculated by difference EIT, by the difference between the current conductivity distribution σ_2 and the reference conductivity distribution σ_1, as presented in Eq. 5 [22].

$$x = \sigma_2 - \sigma_1 \tag{5}$$

The forward problem in difference EIT, i.e. finding the boundary voltage data from the reference conductivity, can be linearly solved by Eq. 6 [22].

$$y = Jx + n \tag{6}$$

where *J* is the Jacobian matrix and *n* is the measurement noise.

A one-step difference GN algorithm was used to solve the EIT inverse problem and for image construction. These approaches can calculate the conductivity as a linear matrix in a fast way, enabling real-time image reconstruction. The one-step GN algorithm looks for the minimized solution $\hat{x}$ of the sum of the quadratic norms as stated in Eq. 7 [22].

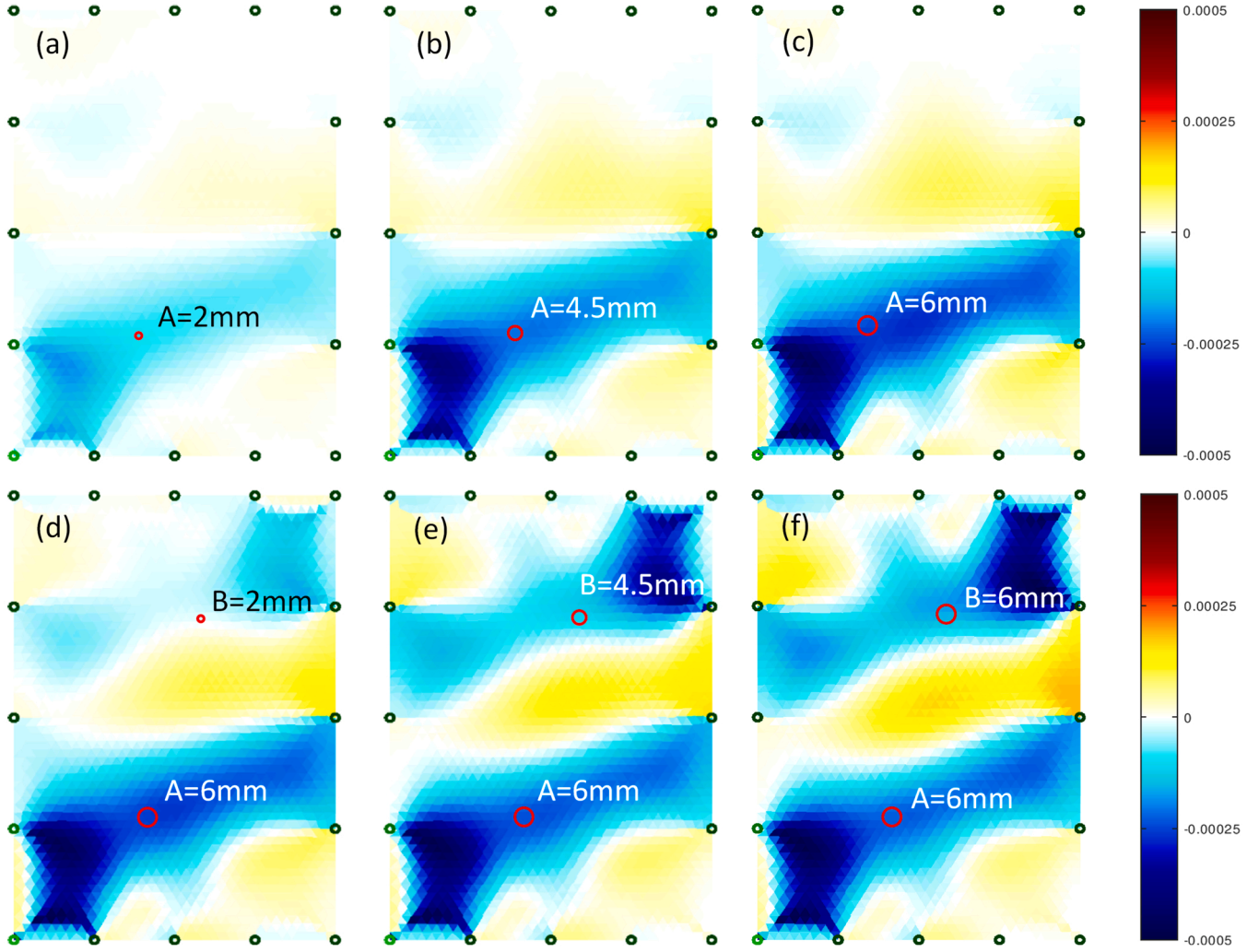

Fig. 5. Reconstructed EIT images using GN algorithm of an unbalanced specimen with through-thickness holes A and B of different diameters: (a) A: 2 mm; (b) A: 4.5 mm; (c) A: 6 mm; (d) A: 6 mm, B: 2 mm; (e) A: 6 mm, B: 4.5 mm; (f) A: 6 mm, B: 6 mm. The green dots represent the connection points of each electrode.

$$\|y - J\hat{x}\|^2_{\sum_n^{-1}} + \|x - x^0\|^2_{\sum_x^{-1}} \tag{7}$$

being x^0 the expected conductivity changes of the element, being zero in difference EIT, $\sum_n$ the covariance matrix from the measurement noise, n, and $\sum_x$ the anticipated image covariance.

The linearized and one-step inverse solution is presented in Eq. 8 [22].

$$\hat{x} = \left(J^T W J + \lambda^2 R\right)^{-1} J^T W y \tag{8}$$

where W and R, given by Eqs. 9 and 10, respectively, are heuristically calculated. R is regularization matrix, and λ is the hyperparameter given by Eq. 11.

$$W = \sigma_n^2 \sum_n^{-1} \tag{9}$$

$$R = \sigma_x^2 \sum_x^{-1} \tag{10}$$

$$\lambda = \frac{\sigma_n}{\sigma_x} \tag{11}$$

being σ_n the average amplitude of the measurement noise and σ_x the initial amplitude of the change in conductivity.

3. Materials and experimental techniques

3.1. Materials

Two different CFRP laminates, having different layup sequences, were produced: an 8-layers quasi-isotropic laminate, with layup sequence [0/45/90/− 45]s, and a 10-layers unbalanced laminate, with layup sequence [0/0/45/90/− 45]s. The laminates were made of a bicomponent epoxy, Biresin® CR83 resin and CH83–6 hardener from Sika AG, Switzerland, in a weight proportion of 100/30 wt%, and unidirectional carbon fibre fabric, 350UT from Toray Industries, Inc., Japan, having a thickness of 0.67 ± 0.10 mm and areal weight of 340 g/m^2. The quasi-isotropic laminate resulted with a thickness of about 2.6 mm and the unbalanced laminate with a thickness of about 3.1 mm.

3.2. Experimental techniques

3.2.1. Production of CFRP laminates

Composite laminates of about 500 mm × 700 mm were manufactured by vacuum assisted resin infusion (VARI). The carbon fibre fabric layers were stacked with the desired orientation in a release agent coated glass plate. Peel ply, for easy demoulding, and flow enhancement medium, to ease resin spreading, were laid on top of the fabric layers. An inlet flow line was installed and connected to the resin container and an outlet resin flow line was connected to a resin catch pot, which was

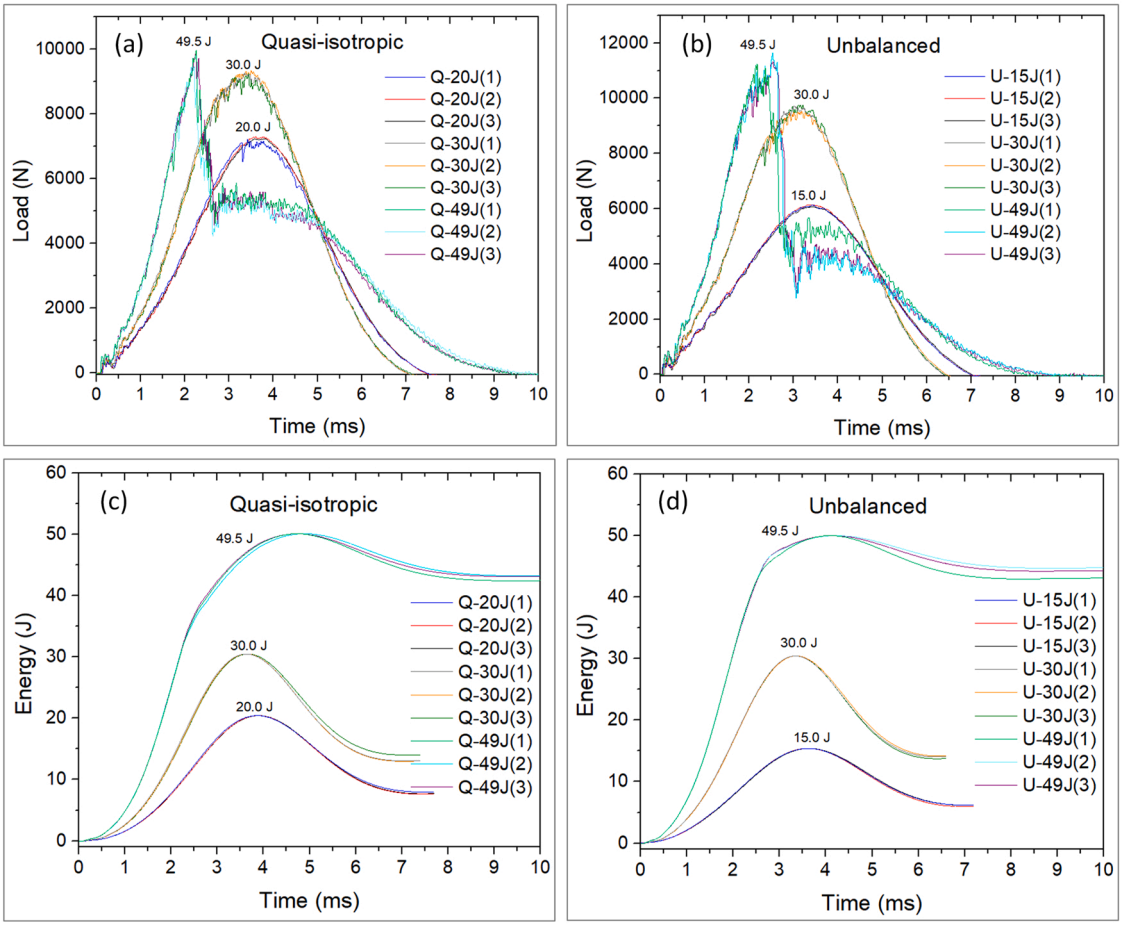

Fig. 6. Impact load vs time curves on (a) quasi-isotropic and (b) unbalanced specimens and respective energy vs time curves (c) and (d).

connected to the vacuum pump. The stacked carbon fibre layers were vacuum bagged to the bottom glass mould using sealing tape. Vacuum was then applied for compaction and air removal. Resin and hardener were mixed following manufacturer's instructions and was let to impregnate the dry carbon fibre preform. The laminates were cured at room temperature under vacuum for about 40 h and post cured at 70 °C for 8 h at ambient pressure. The post-curing process was performed with heating and cooling rates of about 15 °C/h to reduce temperature gradients. The post cured composite plates were cut to obtain several specimens of about 150 × 100 mm, following ASTM D7136 standard, for drop-weight impact testing.

3.2.2. *Introduction of damage in CFRP laminates*

Through-thickness holes were introduced by drilling each composite configuration. Two through-thickness holes per configuration were performed in specific locations of the samples as represented in Fig. 1. The creation of holes followed a specific sequence with EIT imaging being performed between each step. First, hole A was created with an initial diameter of 2 mm and was then increased to 4.5 and 6 mm. The increase of hole diameter aims to assess whether EIT and the GN algorithm are sensitive to damage size. Having hole A with a diameter of 6 mm, hole B was then introduced with the same diameter increase strategy: first a 2 mm diameter followed by a diameter increase to 4.5 and 6 mm. Holes A and B were introduced away from the centre of the sample to avoid mirroring effect.

Impact damages were introduced using drop-weight impact testing. Due to the different layup configurations, the two laminates had distinct impact resistance. Thus, different impact energies had to be imposed on the laminates to produce damages of comparable severity. Different levels of damage severity: unnoticed damage, barely visible damage, and more severe damage, were imposed in the laminates. The quasi-isotropic specimens were subjected to impact energies of 20.0, 30.0 and 49.5 J and the unbalanced specimens to 15.0, 30.0 and 49.5 J. Three specimens of each laminate configuration were exposed to each level of impact energy. Drop-weight impact tests were performed on the Fractovis Plus apparatus from CEAST, following ASTM D7136 standard. The impactor had a 20 mm diameter hemispheric head with a mass of 5.045 kg and its vertical position was adjusted, between 305 and 1000 mm, to impose the distinct levels of impact energy.

3.2.3. *Electrical impedance tomography and ultrasonic inspections*

Sixteen electrodes were applied on the boundary of each specimen, for EIT analysis, as schematically represented by the green circles in Fig. 1. Each sample had an electrode on each corner and 3 electrodes along each edge, spaced about 37 mm on the sample length and 25 mm on the sample width. In order to connect the electrode for measurement to the CFRP sample, first, a silver ink spot was applied on the thickness surface and left to dry for 24 h. Next, a Kapton film was applied on the top surface of the specimen for electrical insulation, where a copper adhesive tape was placed on top of. Electric wires were finally welded. A last layer of glue was used to ensure that the electric wires would not detach during mechanical testing. The boundary electrodes configuration is presented in Fig. 2.

The EIT setup used (Fig. 3) was developed by Stratosphere company. The apparatus consisted of a power supply, XPH 35–4D Dual DC from Sorensen, a 2100 digital multimeter from Keithley, and a type-k thermocouple. The adjacent current injection method was used: the current is injected in a pair of adjacent electrodes and voltage is measured on all

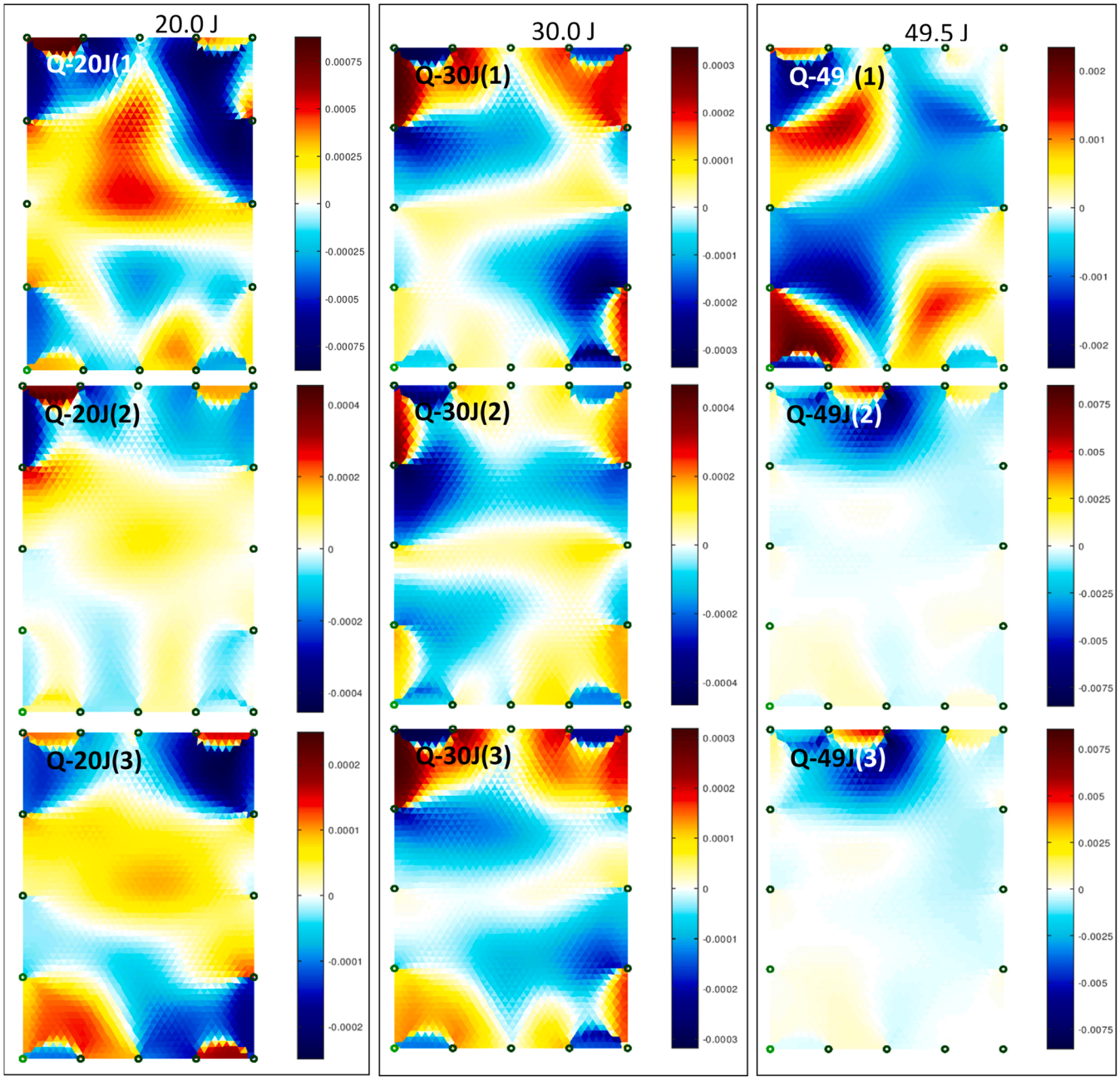

Fig. 7. Reconstructed EIT images using GN algorithm of different quasi-isotropic composite specimens exposed to drop-weight impact events with impact energies of 20.0 J (left), 30.0 J (middle), and 49.5 J (right). The green dots represent the connection points of each electrode.

following adjacent pairs of electrodes. The EIT image reconstruction was processed using an inverse solver with one-step difference GN algorithm, to obtain the difference between specimen condition prior to and after damage introduction. A hyperparameter λ of 1 was used during image reconstruction.

For the EIT measurement on specimens with through-thickness holes, each specimen was analysed by EIT before drilling to serve as reference baseline. Electrical impedance analyses were made on each specimen after each new hole has been created and increased. Regarding impacted specimens, electrical impedance analyses were also carried prior to impact testing, to serve as reference, and after impact testing.

The non-destructive ultrasonic C-scan technique was used to serve as a comparison and validation technique for the suitability of the EIT analysis to detect impact damage. The ultrasonic C-scan analysis were conducted with the Omni Scan Sx from Olympus with a M2008 probe from Olympus, with a frequency of 0.5 MHz. The scans were performed using a two-axis encoder with 1.0 mm resolution in the axis along the length of the samples and 3.0 mm resolution in the axis along the width of the samples.

3.3. Damage analysis

3.3.1. Through-thickness holes

The use of EIT for visible and severe damage detection was evaluated with the introduction of through-thickness holes of different diameters. Figures 4 and 5 show the EIT images of a quasi-isotropic and an unbalanced specimen, respectively, with through-thickness holes A and B with progressive diameter increase from 2 to 6 mm in two locations. Three specimens of each layup configuration were subjected to the same damage, where similar EIT images were obtained.

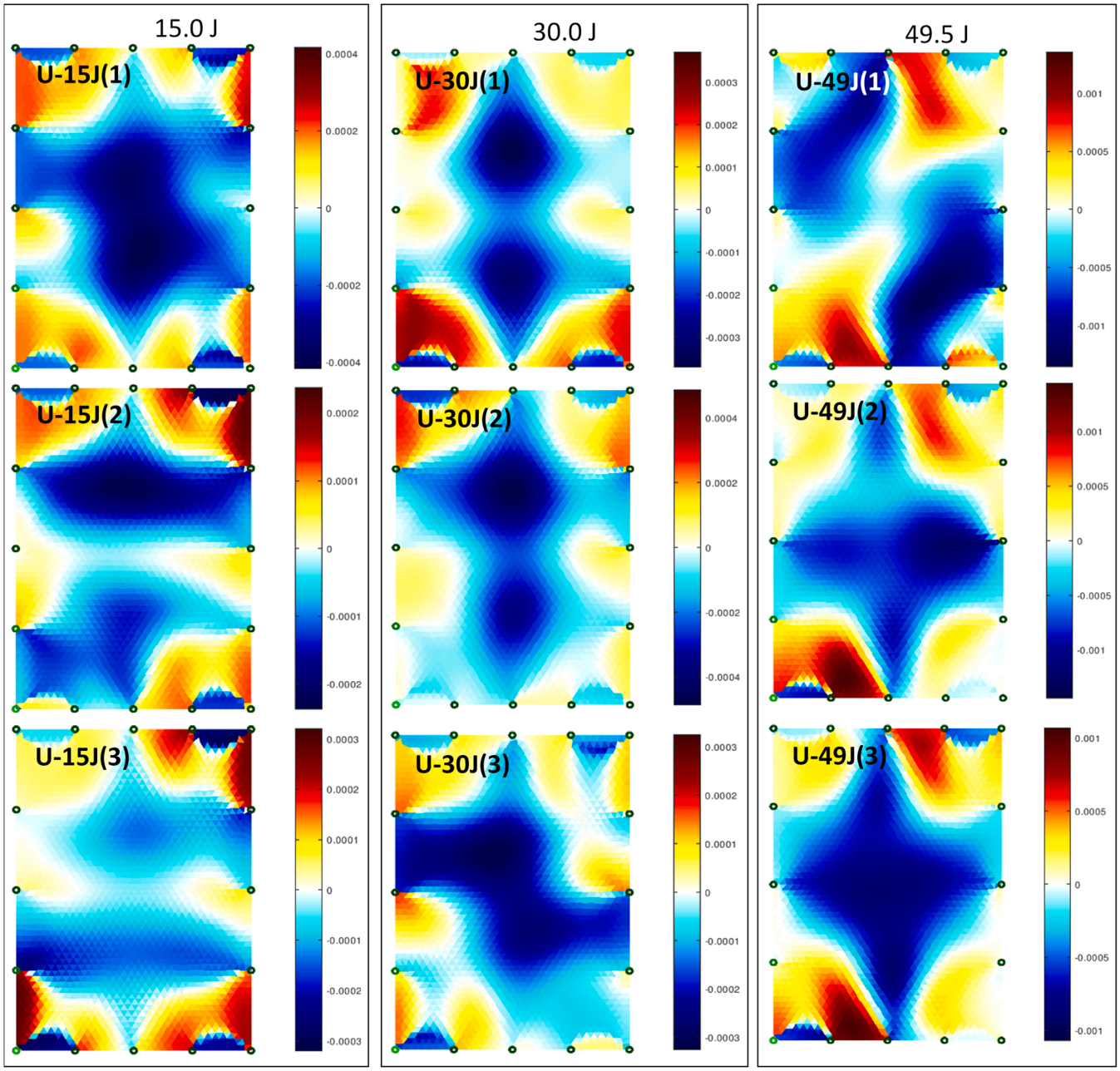

Fig. 8. Reconstructed EIT images using GN algorithm of different unbalanced composite specimens exposed to drop-weight impact events with impact energies of 15.0 J (left), 30.0 J (middle), and 49.5 J (right). The green dots represent the connection points of each electrode.

The damaged locations can be identified by the areas where electrical conductivity was decreased (change of colour towards blue shades). Increasing intensity of the blue colour is observable in the bottom area of Fig. 4 and Fig. 5 (a), (b) and (c), as the diameters of the through-thickness hole A increases. With the introduction of the through-thickness hole B and with the increase of its diameter, an increase of intensity of the blue colour is also observable in the top area of Fig. 4 and Fig. 5 (d), (e) and (f). A decrease of electrical conductivity in the damage sight created an artifact at the closest boundary electrodes, as electrical conduction is affected from the hole location to the boundary electrodes. Yet, the increase of damage severity as the through-thickness hole diameter increases is evident in the reconstructed images. EIT was sensitive to the electrical conductivity changes enforced by the small localized damage imposed by the first through-thickness hole A with a 2 mm diameter. Moreover, the production of hole B did not interfere with the detection of hole A and two distinct damages are clearly observable. The change of electrical conductivity remains constant in the lower part of the image where the through-thickness hole A is found, while the diameter of the through-thickness hole B is being created and then increased. It is possible to see that the real location of the through-thickness holes is at the areas where the different blue zones of lower conductivity, coming from the boundary electrodes converge. In a real engineering application, the exact location of damage could not be indicated, but it would allow to inspect only a rather smaller area of the part to find the damage. These results show the ability of EIT to detect the localized damage and its approximate location, instead of just providing an assessment of the general damage condition in the whole specimen.

3.3.2. *Impact damage*

The contact load and energy recorded by the drop-weight impact testing setup, for the three levels of impact energy are presented in

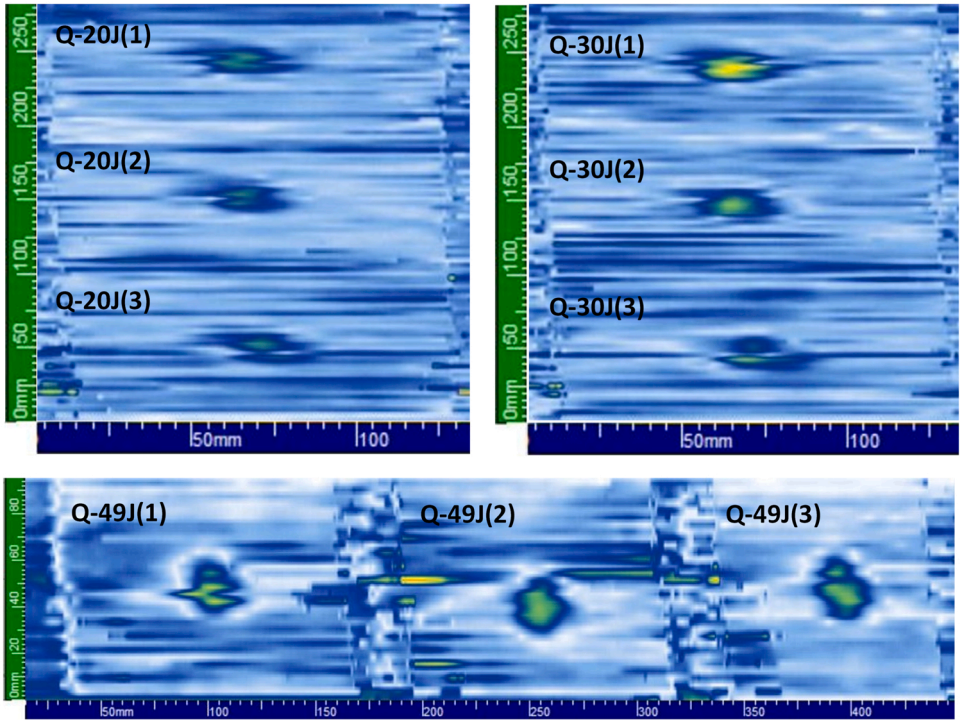

Fig. 9. Ultrasonic C-scan inspection of quasi-isotropic composite specimens exposed to drop-weight impact events with impact energies of 20.0 J (top left), 30.0 J (top right), and 49.5 J (bottom).

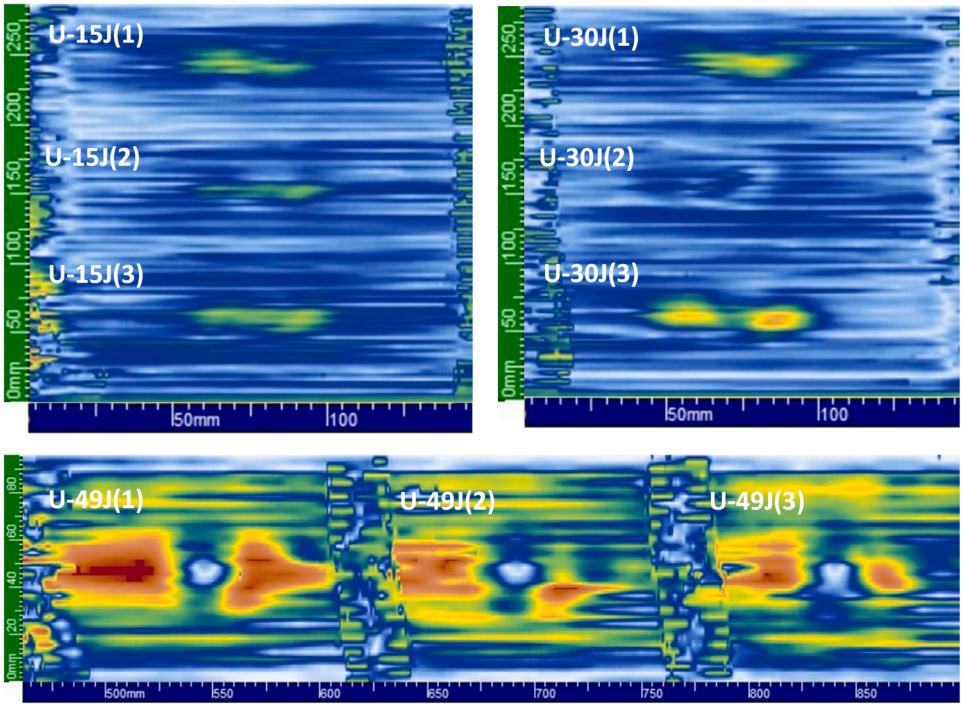

Fig. 10. Ultrasonic C-scan inspection of unbalanced composite specimens exposed to drop-weight impact events with impact energies of 15.0 J (top left), 30.0 J (top right), and 49.5 J (bottom).

Fig. 6. Given the different layup configuration of the two studied laminates and their resultant distinct impact resistance, different impact energies were used to produce unnoticed damage: 20.0 J on quasi-isotropic laminates and 15.0 J on unbalanced laminates. The same levels of impact energies were used on both laminates to produce barely visible damage (30.0 J) and more severe damage (49.5 J). The production of severe damage by impact events with energies of 49.5 J is evident by the sudden decrease of load at around 10,000 N in the case of the quasi-isotropic laminates (Fig. 6(a)) and at around 11,000 N in the case of the unbalanced laminates (Fig. 6(b)) and by the high absorbed energy during impact events, being 85.8 ± 0.7% in the case of the quasi-isotropic laminates (Fig. 6(c)) and 88.3 ± 1.6% in the case of the

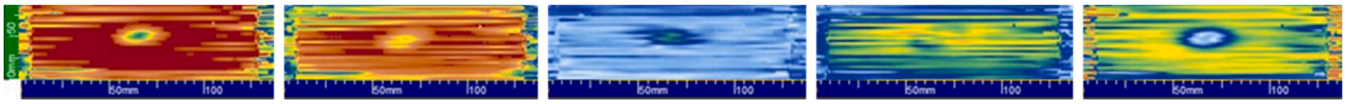

Fig. 11. Ultrasonic C-scan inspection of the quasi-isotropic composite specimen Q-20 J(1) exposed to impact event with energy of 20.0 J at different thickness depth, from left to right: between 2.5 – 2, 2 – 1.5, 1.5 – 1, 1 – 0.5 and 0.5 – 0 mm.

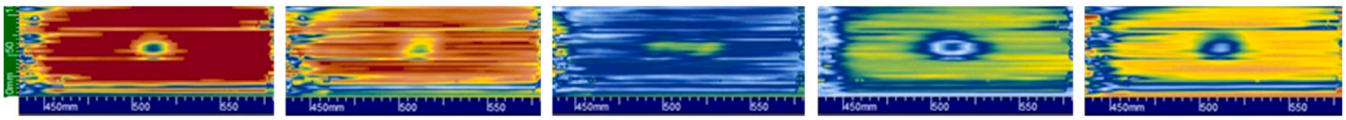

Fig. 12. Ultrasonic C-scan inspection of the unbalanced composite specimen U-15 J(3) exposed to impact event with energy of 15 J at different thickness depth, from left to right: between 2.5 – 2, 2 – 1.5, 1.5 – 1, 1 – 0.5 and 0.5 – 0 mm.

unbalanced laminates (Fig. 6(d)). Both quasi-isotropic and unbalanced laminates submitted to impact events with impact energy of 30.0 J show load oscillations, revealing some degree of imposed damage, with absorbed energies of 43.8 ± 1.5% and 45.9 ± 0.6%, respectively. The impact events of lower impact energy, produced smoother load curves, with the exception of the quasi-isotropic specimen Q-20 J(1), which also showed some load oscillations. The quasi-isotropic laminates absorbed 38.0 ± 0.7% of the impact energy and the unbalanced laminates absorbed 39.9 ± 0.7%.

The EIT images were able to reveal a general different shape of damage in the two laminates with different layup sequences. The quasi-isotropic laminates tend to show a change on the electrical conductivity in the central area of the specimens (Fig. 7). Contrary to what was expected, some samples show an increase of electrical conductivity after damage, with yellowish and reddish regions. Yet, similarly to the tomographic images of specimens with through-thickness holes, a decrease of electrical conductivity is observed from the damaged location towards the boundary electrodes. The unbalanced laminates reveal a change on the electrical conductivity in the central area of the specimens, but with a rather elongated shape (Fig. 8), like the so-called "peanut" shape [7]. The unbalanced specimens consistently present a decrease of electrical conductivity after damage in the "peanut" shape regions, represented in blue colour. The ultrasonic inspections confirmed the shape of damage imposed in the laminates, with the quasi-isotropic laminates showing circular shape-like damages (Fig. 9) and the unbalanced laminates showing elongated shape damages (Fig. 10).

With the EIT technology presenting higher TRL values to evaluate isotropic materials, such as metals, it would be expected that the employment of EIT on quasi-isotropic laminates would yield more accurate results than on the unbalanced laminates. While "peanut" like-shape damage is clearly seen in the unbalanced specimens, the shape of the damages is not evident in the quasi-isotropic laminates, although it is clear that damage is present in the central area of the specimens. The higher number of layers oriented at 0° may contribute to higher electrical conductivity along the surface of the unbalanced samples, yielding more accuracy in damage shape recognition by the EIT technique. The sensitivity of EIT to the presence of damage is highlighted, but it overestimates the area of delaminations, as compared to the ultrasonic C-scan inspections. In the case of unbalanced laminates, the EIT images show damages 1.4–2 times that of damages observed with ultrasounds. While the ultrasound techniques analyse the sound reflection that is dependent on the geometric characteristics of the damage and laminate, the EIT technique evaluates the electrical conductivity, which can be changed not only in the damage area but also around it as current will be scattered and have increased difficulty to pass on.

The slightly shorter impact event duration reveals a more rigid behaviour of unbalanced specimens, when compared to the quasi-isotropic laminates (Fig. 6(a) and (b)). The higher rigidity of the unbalanced laminate is explained by the larger thickness and higher number of layers in the 0° direction, leading to the larger "peanut" shaped delaminations. The damage shape changes across the thickness of the laminate, and the "peanut" shape damage is only observable in the middle layers of the laminate, as it can be seen in Fig. 12 with the example of the specimen U-15 J(3). Therefore, damage detection with EIT technique is independent on the through-thickness location of damage and it can detect the larger damage within the composite. The quasi-isotropic laminates, on the other side, present a rather circular shaped damage throughout the entire thickness of the laminates, as presented in Fig. 11with the example of specimen Q-20 J(1).

4. Conclusions

The use of EIT and the one-step difference GN algorithm for damage detection in carbon fibre composite laminates was evaluated. Different types of damages, through-thickness holes and impact damage of different severities, were inflicted in the composite laminates. Two laminates with different layup configurations, a quasi-isotropic laminate and a highly anisotropic unbalanced laminate, were produced by VARI process.

The EIT was sensitive to the presence of through-thickness holes as small as 2 mm and revealed a gradually larger area with decreased electrical conductivity as the diameter of through-thickness holes increased. It was even possible to identify two distinguished localized damaged areas when two through-thickness holes were present. Similar responses were found for both laminates with different levels of anisotropy.

Each laminate configuration was subjected to three levels of impact energy to create damages with different degrees of severity, unnoticed damage, barely visible damage, and more severe damage. The EIT technique also demonstrated to be able to identify impact damage in the specimens with different levels of anisotropy, with overall distinguished damage shapes. This are encouraging results for the further investigation of EIT for damage detection in real composite parts with different layup configurations. The unbalanced laminate revealed a slightly lower impact resistance, presenting a more rigid behaviour. The impact events on unbalanced specimens produced elongated shaped damages, roughly in the middle layers of the laminate. This elongated "peanut" like-shape damage was revealed by both EIT and ultrasound inspections. The quasi-isotropic specimens had circular shaped damages, as it was revealed by ultrasonic C-scan. However, the EIT images cannot show a well-defined damage shape, but they show changes of electrical conductivity in the central area of the specimens. Overall, the EIT images overestimate the area of damage.

CRediT authorship contribution statement

Helena Rocha: Conceptualization, Writing – original draft,

Methodology, Visualization, Funding acquisition, Project administration. **Christophe Fernandes:** Visualization, Software. **Nelson Ferreira:** Validation. **Ugo Lafont:** Supervision, Writing – review & editing. **João P. Nunes:** Supervision, Writing – review & editing, Funding acquisition.

Declaration of Competing Interest

The authors declare that they have no known competing financial interests or personal relationships that could have appeared to influence the work reported in this paper.

Data Availability

No data was used for the research described in the article.

Acknowledgements

This work was supported by the European Regional Development Fund [grant number NORTE-01-0145-FEDER-000015]; and the European Space Agency [Network/Partnering Initiative Program - ESA Contract 4000123315].

References

[1] V. Giurgiutiu, Structural Health Monitoring of Aerospace Composites, Elsevier, USA, 2016, https://doi.org/10.1016/B978-0-12-409605-9.00001-5.
[2] V. Tita, J. Carvalho, D. Vandepitte, Failure analysis of low velocity impact on thin composite laminates: experimental and numerical approaches, Compos Struct. 83 (2008) 413–428, https://doi.org/10.1016/j.compstruct.2007.06.003.
[3] V. Giurgiutiu, SHM of aerospace composites – challenges and opportunities CAMX Conf. Proc. 2015 1 15.
[4] W.L. Lai, H. Saeedipour, K.L. Goh, Mechanical properties of low-velocity impact damaged carbon fibre reinforced polymer laminates: effects of drilling holes for resin-injection repair, Compos. Struct. 235 (2020), 111806, https://doi.org/10.1016/j.compstruct.2019.111806.
[5] J. Kim, M. Sham, Impact and delamination failure of woven-fabric composites, Compos. Sci. Technol. 60 (2000) 745–761, https://doi.org/10.1016/S0266-3538(99)00166-9.
[6] W.L. Lai, H. Saeedipour, K.L. Goh, Experimental assessment of drilling-induced damage in impacted composite laminates for resin-injection repair: influence of open/blind hole-hole interaction and orientation, Compos. Struct. 271 (2021), 114153, https://doi.org/10.1016/j.compstruct.2021.114153.
[7] S. Abrate, Impact on Composite Structures, Cambridge University Press, 1998.
[8] M. Ramakrishnan, G. Rajan, Y. Semenova, G. Farrell, Overview of fiber optic sensor technologies for strain/temperature sensing applications in composite materials, Sensors 16 (2016) 99, https://doi.org/10.3390/s16010099.
[9] R. Ramly, W. Kuntjoro, M.K.A. Rahman, Using embedded fiber bragg grating (FBG) sensors in smart aircraft structure materials, Procedia Eng. 41 (2012) 600–606, https://doi.org/10.1016/j.proeng.2012.07.218.
[10] B.R. Loyola, V.La Saponara, K.J. Loh, T.M. Briggs, G.O. Bryan, J.L. Skinner, Spatial sensing using electrical impedance tomography, IEEE Sens. J. 13 (2013) 2357–2367.
[11] S. Nonn, M. Schagerl, Y. Zhao, S. Gschossmann, C. Kralovec, Application of electrical impedance tomography to an anisotropic carbon fiber-reinforced polymer composite laminate for damage localization, Compos. Sci. Technol. 160 (2018) 231–236, https://doi.org/10.1016/j.compscitech.2018.03.031.
[12] J. Cagáň, J. Pelant, M. Kyncl, M. Kadlec, L. Michalcová, Damage detection in carbon fiber–reinforced polymer composite via electrical resistance tomography with Gaussian anisotropic regularization, Struct. Heal Monit. (2019) 18, https://doi.org/10.1177/1475921718820013.
[13] T.N. Tallman, S. Gungor, K.W. Wang, C.E. Bakis, Damage detection via electrical impedance tomography in glass fiber/epoxy laminates with carbon black filler, Struct. Heal Monit. 14 (2015) 100–109, https://doi.org/10.1177/1475921714554142.
[14] A.J. Thomas, J.J. Kim, T.N. Tallman, C.E. Bakis, Damage detection in self-sensing composite tubes via electrical impedance tomography, Compos. Part B Eng. (2019) 177, https://doi.org/10.1016/j.compositesb.2019.107276.
[15] A. Baltopoulos, N. Polydorides, L. Pambaguian, A. Vavouliotis, V. Kostopoulos, Damage identification in carbon fiber reinforced polymer plates using electrical resistance tomography mapping, J. Compos Mater. 47 (2013) 3285–3301, https://doi.org/10.1177/0021998312464079.
[16] J. Cagáň, Hardware implementation of electrical resistance tomography for damage detection of carbon fibre–reinforced polymer composites, Struct. Heal Monit. 16 (2017) 129–141, https://doi.org/10.1177/1475921716666004.
[17] J. Cagáň, L. Michalcová, Impact damage detection in CFRP composite via electrical resistance tomography by means of statistical processing, J. Nondestruct. Eval. (2020) 39, https://doi.org/10.1007/s10921-020-00677-2.
[18] A. Baltopoulos, A. Vavouliotis, V. Kostopoulos, N. Polydorides, L. Pambaguian, Electrical tomography as a tool for non-destructive assessment of composite structures. Emerg Technol Non-Destructive Test V - Proc 5th Conf Emerg Technol NDT 2012 389 394 doi: 10.1201/b11837-70.
[19] A. Ampatzoglou, A. Vavouliotis, A. Baltopoulos, V. Kostopoulos, Non destructive evaluation of artificially induced damage in composite structures using electrical resistance/potential mapping. Emerg Technol Non-Destructive Test V - Proc 5th Conf Emerg Technol NDT 2012 381 387 doi: 10.1201/b11837-69.
[20] ASTM D7136/D7136M – 12: Standard test method for measuring the damage resistance of a fiber-reinforced polymer matrix composite to a drop-weight impact event. ASTM Int 2012. https://doi.org/10.1520/D7136.
[21] A. Adler, R. Guardo, Electrical impedance tomography: regularized imaging and contrast detection, IEEE Trans. Med. Imaging 15 (1996) 170–179, https://doi.org/10.1109/42.491418.
[22] A. Adler, T. Dai, W.R.B. Lionheart, Temporal image reconstruction in electrical impedance tomography, Physiol. Meas. (2007) 28, https://doi.org/10.1088/0967-3334/28/7/S01.